

# Uni-PrevPredMap: Extending PrevPredMap to a Unified Framework of Prior-Informed Modeling for Online Vectorized HD Map Construction

Nan Peng  
Ruqi Mobility

pengnan@ruqimobility.com

Xun Zhou  
Ruqi Mobility

zhouxun@ruqimobility.com

Mingming Wang  
GAC R&D Center

wangmingming@gacrnd.com

Guisong Chen  
Ruqi Mobility

chenguisong@ruqimobility.com

Wenqi Xu  
GAC R&D Center

xuwenqi@gacrnd.com

## Abstract

*Safety constitutes a foundational imperative for autonomous driving systems, necessitating maximal incorporation of accessible prior information. This study establishes that temporal perception buffers and cost-efficient high-definition (HD) maps inherently form complementary prior sources for online vectorized HD map construction. We present Uni-PrevPredMap, a pioneering unified framework systematically integrating previous predictions with corrupted HD maps. Our framework introduces a tri-mode paradigm maintaining operational consistency across non-prior, temporal-prior, and temporal-map-fusion modes. This tri-mode paradigm simultaneously decouples the framework from ideal map assumptions while ensuring robust performance in both map-present and map-absent scenarios. Additionally, we develop a tile-indexed 3D vectorized global map processor enabling efficient 3D prior data refreshment, compact storage, and real-time retrieval. Uni-PrevPredMap achieves state-of-the-art map-absent performance across established online vectorized HD map construction benchmarks. When provided with corrupted HD maps, it exhibits robust capabilities in error-resilient prior fusion, empirically confirming the synergistic complementarity between temporal predictions and imperfect map data. Code is available at <https://github.com/pnnnnnnn/Uni-PrevPredMap>.*

## 1. Introduction

High-Definition (HD) maps serve as critical infrastructure for autonomous vehicles, delivering centimeter-level road geometry and semantic information to ensure precise localization and safe navigation. These maps can be generated through two primary approaches: traditional offline

SLAM-based mapping workflows or emerging online perception systems. Given the prohibitive costs associated with offline HD map production and maintenance, the automotive industry is increasingly prioritizing online vectorized HD map construction techniques [13, 19].

Online vectorized HD map construction experiences reliability degradation when onboard sensors encounter visual deprivation scenarios, including severe occlusion environments and beyond-visual-range conditions. To address these limitations, researchers have proposed utilizing two prior sources: temporal perception buffers and cost-efficient HD maps (e.g., less frequently updated HD maps and crowd-sourced HD maps). The two prior sources exhibit inherent complementarity: temporal buffers ensure backward continuity through sequential observation accumulation, while cost-efficient HD maps establish forward-looking constraints via predefined geometry structures. However, existing prior-informed models remain limited to processing either temporal perception buffers [3, 15, 29, 34, 40, 42] or cost-efficient HD maps [14, 32] in isolation, as depicted in Figure 1 (a). Consequently, designing a unified framework compatible with both priors is crucial to fully leverage their strengths and enhance performance for safety-critical autonomous systems.

Integrating temporal perception buffers with cost-efficient HD map priors presents two fundamental challenges: (1) Cost-efficient HD maps are prone to errors, including false positives, false negatives, and pose misalignment. Current HD map prior models shown in Figure 1 (b), however, tend to over-rely on idealized fidelity assumptions [1], causing potential ground truth leakage. To mitigate this, the unified framework must actively detect map errors rather than implicitly trust flawed priors. (2) Cost-efficient HD maps inevitably contain uncovered regions. Consequently, the unified framework must exhibit robust standalone perception capabilities in map-absent areas, while

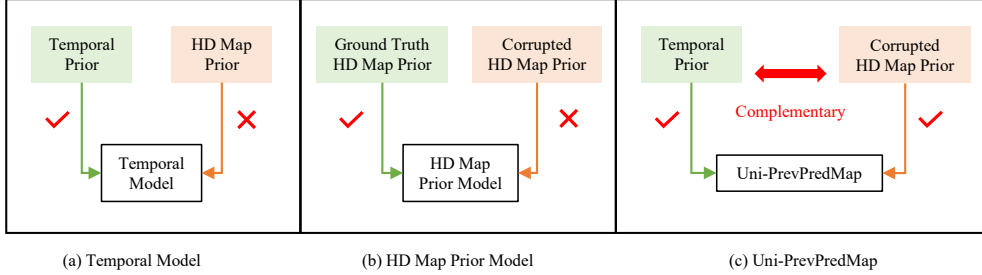


Figure 1. Motivation of Uni-PrevPredMap. (a) Existing prior-informed models are constrained to handling temporal perception buffers or cost-efficient HD maps separately. (b) Current HD map prior models tend to over-rely on idealized fidelity assumption. (c) Uni-PrevPredMap delivers robust standalone perception in map-absent areas while boosting reliability in map-present areas through adaptive fusion coupled with active map error identification.

simultaneously enhancing reliability in map-present areas through adaptive fusion.

In this work, we present Uni-PrevPredMap, extending the temporal baseline PrevPredMap [29], as a unified prior-informed framework for online vectorized HD map construction. Our approach explores the previously untapped synergy between two complementary prior sources: previous predictions and corrupted HD maps. To address existing challenges, we introduce a tri-mode paradigm employing stratified sampling across non-prior, temporal-prior, and temporal-map-fusion modes during training, where map priors undergo instance-level perturbation. This simple but effective paradigm simultaneously decouples the model from ideal map assumptions while enabling robust performance in both map-absent and map-present scenarios. Furthermore, we incorporate a novel tile-indexed 3D vectorized global map processor enabling efficient 3D prior updates, compact storage, and real-time retrieval. This processor uses geolocation-specific tile partitioning synchronized with vehicle positioning to eliminate complex post-processing. The solution extends existing 2D rasterized [42] and vectorized [31] approaches into full 3D vectorization, enhancing real-world applicability.

In summary, the contributions of this work include: (1) We establish that temporal perception buffers and cost-efficient HD maps serve as complementary priors for online vectorized HD map construction. Based on this foundational insight, we propose Uni-PrevPredMap, the first unified framework to strategically integrate previous predictions with corrupted HD maps. (2) A tri-mode paradigm is introduced to preserve operational consistency across non-prior, temporal-prior, and temporal-map-fusion modes, simultaneously decoupling Uni-PrevPredMap from ideal map assumptions while maintaining robust performance in both map-absent and map-present scenarios. (3) A tile-indexed 3D vectorized global map processor is developed to enable efficient 3D prior data refreshment, compact storage, and

real-time retrieval. (4) Uni-PrevPredMap achieves state-of-the-art map-absent performance across established online vectorized HD map construction benchmarks. When processing corrupted HD maps, it demonstrates robust error-resilient prior fusion capabilities, empirically confirming the synergistic complementarity between temporal predictions and cost-efficient HD maps.

## 2. Related Work

Online vectorized HD map construction was initially conceptualized as a semantic segmentation problem [4, 16, 18, 28]. HDMaNet [16] established a raster-to-vector conversion pipeline that first generates BEV semantic segmentation maps and subsequently groups these pixel-wise results into vectorized instances through heuristic post-processing. VectorMapNet [23] introduced the first end-to-end framework, utilizing an auto-regressive transformer architecture for sequential vector instance retrieval. MapTR [19] subsequently revolutionized this domain through a unified permutation-equivalent representation and hierarchical query embedding scheme, achieving one-stage parallel decoding that significantly enhanced computational efficiency. Recent advancements demonstrate following innovation directions, including concise map representations [6, 17, 21, 30, 43, 44], optimized attention mechanisms [10, 20, 38], structural query designs [24, 38], multi-modal distillation [8], and segmentation-based auxiliary supervision [5, 20, 22, 26].

### 2.1. Online Vectorized HD Map Construction with Temporal Perception Buffers

Runtime temporal perception information inherently exists without supplementary acquisition overhead. In temporal modeling methodologies, StreamMapNet [40] implements dense-sparse feature co-fusion through streaming integration of BEV and query features. SQD-MapNet [34] advances this paradigm by introducing a stream query de-

noising strategy to facilitate temporal consistency learning. MapTracker [3] and MapUnveiler [15] leverage memory buffers to integrate previous BEV and query features, achieving temporal fusion at the feature level. In contrast, PrevPredMap [29] pioneers a prediction-level temporal modeling approach, implying distinct advantages for seamless map integration. Building upon this foundation, Uni-PrevPredMap extends PrevPredMap [29] into a unified framework that effectively incorporates two complementary prior sources: historical predictions and imperfect HD maps.

Generally, map elements exhibit static properties. Map features or predictions perceived at location X can serve as prior whenever the road structure near X remains unchanged. Building on this observation, NMP [37] and NeMO [45] develop region-centric approaches that leverage temporal information. PreSight [41] introduces Neural Radiance Fields (NeRF) to alleviate memory constraints and generate city-scale priors. HRMapNet [42] employs a global map processor that stores and distributes rasterized historical predictions. Uni-PrevPredMap redesigns this component into a tile-indexed 3D vectorized representation. This redesign achieves three key improvements: (1) elevating the representation from 2D to 3D, (2) reducing storage overhead by shifting from rasterization to vectorization, and (3) enhancing retrieval efficiency through tile-based indexing. This processor is central to our framework, maintaining global state for both temporal buffer and corrupted maps.

## 2.2. Online Vectorized HD Map Construction with Cost-efficient Alternative Maps

Cost-efficient maps provide critical priors for online vectorized HD map construction. Multiple prior categories have been explored, including Standard Definition (SD) maps [14, 25, 36], HD maps [14, 32], and satellite imagery [7]. Although SD maps are widely available, they lack granular semantics required for safety-critical autonomy. These maps cannot encode essential divider attributes like color and type, nor can they represent pedestrian crossings, stop lines, directional arrows, or elevation data. While cost-efficient HD maps present higher accessibility barriers than SD maps, their operational feasibility remains proven: major OEMs routinely maintain lightweight HD maps containing basic lane geometry and safety-critical elements. However, current HD map prior models often rely heavily on idealized map assumptions, leading to significant performance degradation when processing erroneous map data [1], a phenomenon that suggests potential ground truth leakage. In contrast to these methods, which assume that the prior map is geometrically accurate, semantically complete, and fully covering the operational area, Uni-PrevPredMap is designed to be robust to these deviations. It effectively handles geometric noise, missing or extraneous map el-

ements, and uncovered regions, thereby reducing dependence on ideal map conditions.

## 3. Method

### 3.1. Overall Architecture

Uni-PrevPredMap retains PrevPredMap’s core architectural principle of prediction-driven temporal modeling instead of feature-level processing, enabling native map prior assimilation. Figure 2 illustrates the overall architecture. Surrounding multi-view images are processed through an image encoder to extract features. Concurrently, the tile-indexed 3D vectorized global map processor retrieves temporal and map priors using vehicle positioning coordinates. Through the tri-mode paradigm, these priors are processed into non-prior, temporal-prior, or temporal-map-fusion configurations based on the selected mode. The processed priors then combine with image features via the BEV encoder to generate prior-augmented BEV features while simultaneously initializing queries. These prior-informed BEV and query features are subsequently decoded into final map predictions that undergo incremental updates within the tile-indexed 3D vectorized global map processor.

### 3.2. Tri-mode Paradigm

We introduce a tri-mode paradigm ensuring operational robustness across non-prior, temporal-prior, and temporal-map-fusion modes. Through instance-level perturbation applied to map priors, this tri-mode paradigm simultaneously decouples the model from ideal map assumptions while enabling consistent performance in both map-absent and map-present scenarios.

As illustrated in Figure 2 and Algorithm 1 (appendix), retrieved 3D vectors first undergo spatial filtering constrained by intersection with the predefined perception range. Crucially, 2D vectors inherently lack vertical differentiation capability, preventing distinction of multi-level configurations like elevated overpasses and subterranean tunnels that risk propagating erroneous priors. During training, instance-level perturbation is applied to filtered map priors, where random vector subsets receive distinct displacement magnitudes sampled uniformly from [0,6] meters. This stochastically displaces approximately half of map vectors with mean 3-meter displacement, aligning with standard lane widths. The process simulates real-world infrastructure modifications including divider adjustments, boundary changes, and pedestrian crossing relocation. During inference, Uni-PrevPredMap’s robustness is tested against untrained perturbations including instance-level addition/deletion and frame-level displacement/rotation/scaling operations, with detailed definitions and visualizations in Appendix A.1. Finally, rasterization generates temporal, map, and empty priors.

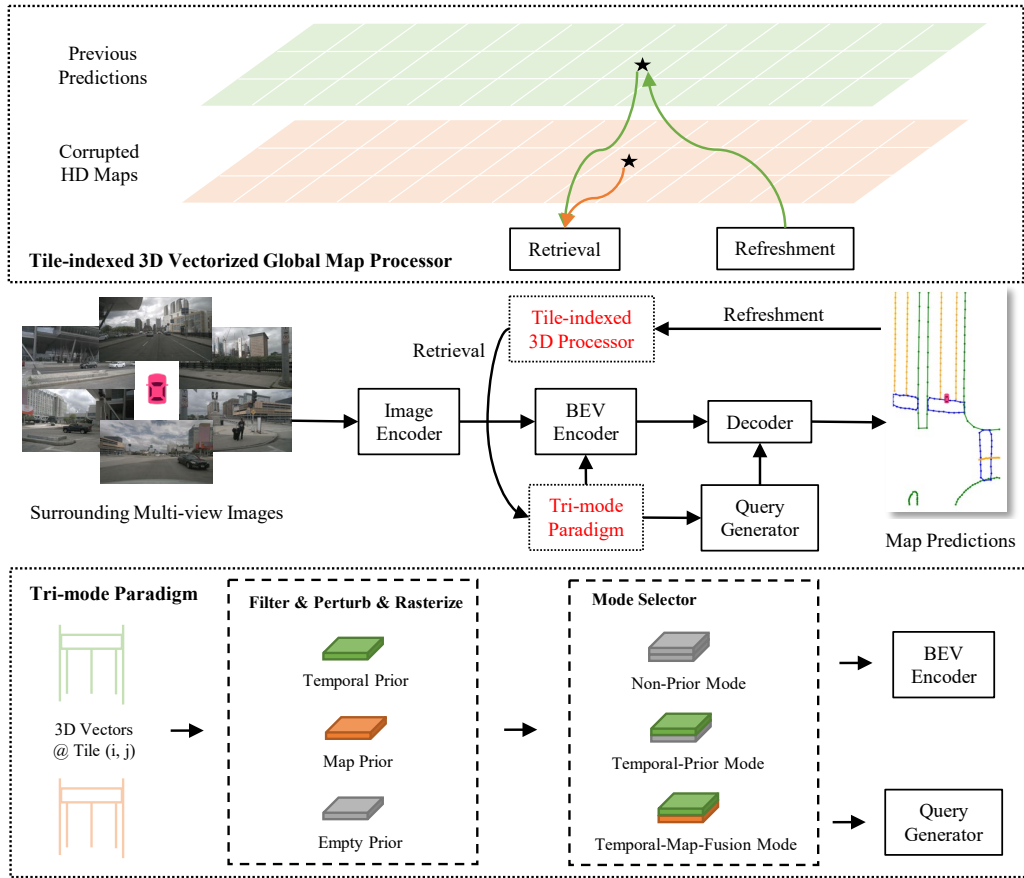


Figure 2. The overall architecture of Uni-PrevPredMap. The upper dashed region highlights the tile-indexed 3D vectorized global map processor enabling efficient 3D prior data refreshment, storage, and retrieval. The lower dashed region outlines the tri-mode paradigm ensuring consistent operation across non-prior, temporal-prior, and temporal-map-fusion modes.

According to the selected operational mode, temporal, map, and empty priors are combined pairwise before concatenation as shown in Figure 2. During training, Uni-PrevPredMap employs a stratified sampling strategy across three distinct modes: non-prior, temporal-prior, and temporal-map-fusion. These modes are sampled according to a fixed ratio. In the temporal-map-fusion mode, map vectors are retrieved from both the temporal buffer and corrupted map of the global map. These vectors are rasterized into temporal and map heatmaps before being processed by the BEV encoder and query generator. The temporal-prior mode uses only vectors from the temporal buffer to generate the temporal heatmap, while the map heatmap is set to a zero matrix. In the non-prior mode, both heatmaps are initialized as zero matrices. This tri-mode design enables seamless switching during inference based on the availability of cost-effective HD maps. The system adaptively activates the temporal-map-fusion mode when operating continuously within a mapped area with both temporal buffer

and map data available. The temporal-prior mode is triggered upon entering a region with no map coverage, relying solely on the temporal buffer. The non-prior mode serves as a fallback when both the temporal buffer is unavailable (e.g., after a system restart) and map data is absent.

Processed priors then follow two parallel processing pathways: (1) The BEV encoder concatenates priors with BEV features using HRMapNet’s approach [42], followed by convolutional layer fusion; (2) The query generator employs deformable attention where priors function as keys/values for spatial interaction with map queries.

### 3.3. Tile-indexed 3D Vectorized Global Map Processor

We propose a tile-indexed 3D vectorized global map processor that eliminates complex post-processing through geolocation-synchronized tile partitioning, enabling efficient 3D prior updates, compact storage, and real-time retrieval. Specifically, the tile-indexed processor implements

dual-axis geospatial indexing where each (i,j)-indexed tile defines a bounded geographical region containing discrete map vectors confined to respective tile boundaries.

**Refreshment** selectively integrates high-confidence predictions into ego-pose-associated tiles of the global map, with detailed mapping in Appendix A.2. For previous predictions, predicted vectors are updated to specified tiles, whose indices are calculated using the vehicle’s UTM (Universal Transverse Mercator) coordinates. For corrupted HD maps, global vectors are pre-stored in corresponding indexed tiles for target regions, with tile indices derived from the map vector’s UTM coordinates.

**Retrieval** queries relevant map elements from specific tiles anchored to the ego pose. Temporal and map priors are retrieved from target tiles indexed via the vehicle’s UTM coordinates, leveraging the refreshment mapping described above. To ensure data integrity, adjacent tiles surrounding the target tile are concurrently retrieved, with detailed visualizations and mapping in Appendix A.2.

## 4. Experiment

### 4.1. Experimental Setup

**Datasets** We evaluate Uni-PrevPredMap on two popular and large-scale datasets: nuScenes [2] and Argoverse2 [35]. The nuScenes dataset offers 2D vectorized maps alongside 1000 scenes, with 700 designated for training and 150 for validation. Each scene encompasses 20 seconds of 2Hz RGB images captured by 6 cameras. Argoverse2, on the other hand, delivers 3D vectorized maps and consists of 1000 logs, with 700 allocated for training and 150 for validation. Each log comprises 15 seconds of 20Hz RGB images from 7 ring cameras.

**Evaluation Metrics** Consistent with previous methods [16, 19, 23], we select three static map categories for a fair evaluation: pedestrian crossings, lane dividers, and road boundaries. The perception range is set as 30m front and rear and 15m left and right of the vehicle. The common average precision (AP) based on Chamfer Distance is used as the evaluation metric under 3 thresholds of {0.5, 1.0, 1.5}m.

**Implementation Details** We utilize ResNet50 [9] as the perspective backbone and LSS-based BEVPoolv2 [12] as the parameterized PV-to-BEV transformation network. The optimizer is AdamW with a weight decay 0.01, and the initial learning rate is set to 0.0006, employing a cosine decay schedule. The batch size is 16 and all models are trained with 4 NVIDIA A100 GPUs. We define the size of each BEV grid as 0.3 meters. The default numbers of instance

queries, point queries and decoder layers are 100, 20 and 6, respectively.

### 4.2. Comparisons with State-of-the-art Methods

**Performance on nuScenes** As shown in Table 1, Uni-PrevPredMap achieves 74.0 mAP (24-epoch training) and 77.0 mAP (72-epoch training), surpassing all SOTA methods in training convergence, validation accuracy, and inference speed. When integrated with corrupted HD maps, the enhanced variant Uni-PrevPredMap\* attains 80.9 mAP (24-epoch) and 81.8 mAP (72-epoch), demonstrating stable performance under map degradation. While Uni-PrevPredMap demonstrates strong overall performance, it does not surpass every state-of-the-art method across all metrics, particularly in boundary and pedestrian crossing. Under the map-absent setting, Uni-PrevPredMap achieves a Boundary AP that is 0.7 lower than Mask2Map [5]. We attribute this primarily to the difference in conditioning strategies: Mask2Map [5] utilizes the segmentation heatmap of the current frame as prior, which provides highly precise and up-to-date spatial information. This proves particularly advantageous for modeling boundaries, which tend to exhibit significant inter-frame variation. In contrast, our approach relies on historical heatmaps, leading to a slight decrease in Boundary AP in the absence of a map. When a corrupted map prior is provided, Uni-PrevPredMap surpasses Mask2Map [5] by a significant margin of 5.0 AP. In the case of pedestrian crossings, Uni-PrevPredMap underperforms MapTracker [3] by 2.1 AP under the map-absent setting. This can be explained by the fact that pedestrian crossings are less structured and more challenging to reconstruct from rasterized heatmaps compared to dividers and boundaries. MapTracker [3] leverages historical query features that preserve vector-level semantics, thereby reducing the modeling difficulty for such elements. However, when a noisy map prior is introduced, the performance gap narrows to just 0.3 AP. Inspired by these two observations, we identify two promising directions for future work: incorporating the segmentation heatmap of the current frame to enhance spatial precision, and integrating vector-level semantic features to better model unstructured elements. Any such enhancements, however, must carefully balance the potential performance gains against the increase in inference latency caused by added model complexity.

**Performance on Argoverse 2** Argoverse2 provides a 3D vectorized map containing additional elevation data, addressing the vertical dimension information lacking in the nuScenes dataset. As demonstrated in Table 2, comparative evaluations under 3D evaluation configurations reveal performance characteristics. Following the experimental protocol established by MapTRv2, we trained Uni-PrevPredMap over 6 epochs and evaluated it at a 2.5Hz

Table 1. Comparison with SOTA methods on nuScenes. All backbones utilized are ResNet50. FPS measurements are conducted on the same machine with NVIDIA RTX A6000. \* are taken from the corresponding papers and are scaled based on the FPS of MapTRv2 [20].

Method	Epoch	$AP_{div}$	$AP_{ped}$	$AP_{bou}$	mAP	FPS
MapTRv2 [20]	24	62.4	59.8	62.4	61.3	16.4
HRMapNet [42]	24	67.4	65.8	68.5	67.2	13.3
Mask2Map [5]	24	71.3	70.6	72.9	71.6	9.5
MapTracker [3]	24	69.2	75.3	71.2	71.9	11.7
MapUnveiler [15]	24	67.6	67.6	68.8	68.0	13.4*
PriorMapNet [33]	24	69.0	64.0	68.2	67.1	13.7*
FastMap [11]	24	69.1	65.5	69.7	68.1	17.2*
Uni-PrevPredMap	24	<b>72.3</b>	<b>76.2</b>	<b>73.6</b>	<b>74.0</b>	12.2
Uni-PrevPredMap*	24	84.1	79.1	79.6	80.9	11.5
MapTRv2 [20]	110	68.8	68.0	71.0	69.2	16.4
HIMap [44]	110	75.0	71.3	74.7	73.7	10.0*
HRMapNet [42]	110	72.9	72.0	75.8	73.6	13.3
Mask2Map [5]	110	73.6	73.1	<b>77.3</b>	74.6	9.5
MapTracker [3]	72	74.1	<b>80.0</b>	74.1	76.1	11.7
MGMapNet [39]	110	74.3	71.8	74.8	73.6	13.3*
Uni-PrevPredMap	72	<b>76.3</b>	77.9	76.6	<b>77.0</b>	12.2
Uni-PrevPredMap*	72	83.4	79.7	82.3	81.8	11.5

Table 2. Comparison with SOTA methods on Argoverse2. All backbones utilized are ResNet50.

Method	$AP_{div}$	$AP_{ped}$	$AP_{bou}$	mAP
MapTRv2 [20]	68.9	60.7	64.5	64.7
HIMap [44]	68.3	66.7	70.3	68.4
MapUnveiler [15]	72.6	66.0	67.6	68.7
MGMapNet [39]	72.1	64.7	70.4	69.1
PriorMapNet [33]	73.4	66.5	69.8	69.9
Uni-PrevPredMap	<b>74.5</b>	<b>69.5</b>	<b>72.9</b>	<b>72.3</b>
Uni-PrevPredMap*	82.5	75.2	80.5	79.4

sampling rate. The results in Table 2 indicate that Uni-PrevPredMap achieves 72.3 mAP, outperforming all SOTA methods in 3D vectorized HD map construction on the Argoverse2 benchmark. While Uni-PrevPredMap\*, enhanced through integration with corrupted HD maps, achieves superior performance with 79.4 mAP.

### 4.3. Ablation Study

**Framework Evolution: PrevPredMap to Uni-PrevPredMap** Based on PrevPredMap [29], we incrementally introduce a tile-indexed 3D vectorized global map processor and tri-mode paradigm, with results detailed in Table 3. The 3D processor enables multi-frame historical predictions to inform the model through both BEV encoder and query generator pathways, extending beyond PrevPredMap’s single-frame query attention mechanism.

This advancement increases map-absent performance from 66.3 to 74.0 mAP. Crucially, the tri-mode paradigm unlocks robust map usage, elevating performance to 80.9 mAP with a map prior while maintaining the 74.0 mAP competitive performance without it. This demonstrates that our model gains a significant advantage when a map is available, without any degradation when it is absent.

### Comparative Performance across Tri-mode Paradigm Variants

Table 4 systematically explores degraded variants of the proposed tri-mode paradigm. The single-mode variant trains exclusively under map-prior conditions, while dual-mode configurations include dual-mode-a (non-prior and map-prior modes) and dual-mode-b (temporal-prior and temporal-map-fusion modes). As shown, the single-mode approach, which is typical in existing HD map prior models [14, 32], collapses in map-absent scenarios. We emphasize that robust map-absent perception capability serves as a necessary condition to prevent ground truth leakage. Performance gaps reveal critical dependencies: the 13.4 mAP deficit in temporal-deprived dual-mode-a demonstrates synergistic necessity between temporal buffers and cost-efficient HD maps, whereas the 5.0 mAP shortfall in dual-mode-b underscores integrated adaptability’s indispensability. Essentially, the tri-mode paradigm proves pivotal by liberating models from idealized map assumptions while achieving state-of-the-art map-absent performance and significantly boosting accuracy with cost-efficient HD maps. These advances address core challenges in online

Table 3. Framework evolution: PrevPredMap to Uni-PrevPredMap.

Setting	mAP (w/o map)	mAP (w/ map)
PrevPredMap	66.3	-
+ tile-indexed 3D vectorized global map processor	74.0	-
+ tri-mode paradigm	74.0	80.9
= Uni-PrevPredMap	+7.7	+80.9

Table 4. Comparative performance across tri-mode paradigm variants.

Training Paradigm	mAP (w/o map)	mAP (w/ map)
Single-mode	16.6	82.9
Dual-mode-a	60.6	77.4
Dual-mode-b	69.0	84.4
Tri-mode	74.0	80.9

Table 5. Inference performance under different prior conditions.

Temporal Prior	Map Prior	mAP	FPS
×	×	64.9	14.2
✓	×	74.0	12.2
×	✓	71.3	13.1
✓	✓	80.9	11.5

vectorized HD map construction: maintaining robust standalone operation in map-absent regions and enhancing reliability through active map error identification in map-present areas.

**Inference Performance under Different Prior Conditions** Table 5 demonstrates that our tri-mode paradigm ensures consistent robustness across map-absent (74.0 mAP) and map-present (80.9 mAP) scenarios. Combined temporal and map priors (80.9 mAP) significantly outperform individual priors (temporal: 74.0 mAP; map: 71.3 mAP), confirming their complementary role in enhancing perception stability through temporal buffering and HD map constraints.

**Robustness to Artificial HD Map Perturbations** Uni-PrevPredMap is trained with instance-level displacement uniformly sampled from  $[0, 6\text{m}]$ , while more unseen perturbations are applied during inference to simulate real-world corruption and test robustness. Specifically, we implement instance-level addition/deletion and frame-level displacement/rotation/scaling operations, with detailed definitions and visualizations in Appendix A.1. As Table 6 shows, even

Table 6. Robustness to artificial HD map perturbations (Inst. = Instance-level, Frame = Frame-level).

Type	Noise Range	mAP
Perfect Map	-	85.6
Inst. Displacement	$[-3\text{m}, 3\text{m}]$	81.9
	$[-6\text{m}, 6\text{m}]$	80.9
	$[-9\text{m}, 9\text{m}]$	80.3
Inst. Addition	$[0, 10]$	85.2
Inst. Deletion	$[0, 10]$	82.5
Frame Displacement	$[-3\text{m}, 3\text{m}]$	77.0
	$[-6\text{m}, 6\text{m}]$	75.7
	$[-9\text{m}, 9\text{m}]$	74.6
Frame Rotation	$[-15^\circ, 15^\circ]$	77.0
Frame Scale	$[0.8, 1.2]$	77.0
Empty Map	-	74.0

with perfect maps, Uni-PrevPredMap achieves 85.6 mAP, significantly below perfect accuracy, indicating it leverages map priors through map-absent perception capability (74.0 mAP) rather than memorizing ground truth. Performance adaptively adjusts to displacement ranges: smaller deviations show improvement while larger ones cause deterioration. Instance-level addition and deletion respectively simulate road removals and unmapped constructions, with Uni-PrevPredMap demonstrating exceptional resilience (merely 0.4 mAP drop for additions, controlled 3.1 mAP drop for deletions). We emphasize that HD map prior models must discriminatively leverage both existence and non-existence evidence to enhance reliable cues while suppressing erroneous ones, thereby optimizing scene understanding. For frame-level perturbations where all map vectors uniformly deviate from temporal observations, Uni-PrevPredMap maintains robustness against corrupted HD maps, outperforming map-absent baselines. This resilience likely stems from cross-validation mechanisms between temporal observations and map constraints that effectively mitigate erroneous prior impacts.

**Ablation on the Sampling Ratio of the Tri-mode Paradigm** During training, Uni-PrevPredMap employs

Table 7. Ablation on the tri-mode sampling ratio with T:T&M fixed at 3:2 on nuScenes. "N", "T", and "M" denote non-prior, temporal prior, and map prior respectively.

Ratio (N:T:T&M)	mAP (T)	mAP (M)	mAP (T&M)
0.30 : 0.42 : 0.28	73.4	72.4	82.7
0.40 : 0.36 : 0.24	73.7	71.8	82.0
0.50 : 0.30 : 0.20	74.0	71.3	80.9
0.60 : 0.24 : 0.16	73.9	70.3	79.7
0.70 : 0.18 : 0.12	72.7	69.4	78.0

Table 8. Ablation on the tri-mode sampling ratio with N:(T+T&M) fixed at 1:1 on nuScenes.

Ratio (N:T:T&M)	mAP (T)	mAP (M)	mAP (T&M)
0.50 : 0.35 : 0.15	73.1	69.8	79.4
0.50 : 0.30 : 0.20	74.0	71.3	80.9
0.50 : 0.25 : 0.25	73.6	72.0	81.4
0.50 : 0.50 : 0.00	74.0	-	-

Table 9. Ablation on the tri-mode sampling ratio with N:(T+T&M) fixed at 1:1 on ArgoVerse2.

Ratio (N:T:T&M)	mAP (T)	mAP (M)	mAP (T&M)
0.50 : 0.35 : 0.15	71.5	72.9	77.8
0.50 : 0.30 : 0.20	72.4	73.6	78.6
0.50 : 0.25 : 0.25	72.3	74.7	79.4
0.50 : 0.50 : 0.00	71.9	-	-

stratified sampling across non-prior, temporal-prior, and temporal-map-fusion modes. We performed ablations from two perspectives. First, with the ratio between temporal-prior (T) and temporal-map fusion (T&M) modes fixed at 3:2, we varied the proportion of the non-prior mode (N) to the combined prior-based modes (T+T&M). As shown in Table 7, the best map-absent performance was achieved at N:(T+T&M) = 0.5:0.5. Reducing the proportion of (T+T&M) led the model to overfit the non-prior scenario, degrading performance in both temporal-prior and fusion-prior settings. Conversely, increasing (T+T&M) resulted in over-reliance on priors: while fusion-prior performance improved slightly, temporal-prior performance declined. This may be attributed to the fact that temporal-prior inference still relies on an initial non-prior prediction; weakening that foundation adversely affects subsequent predictions. Second, with N:(T+T&M) fixed at 1:1, we varied the T:T&M ratio on both nuScenes (Table 8) and ArgoVerse2 (Table 9). The results showed consistent trends across datasets,

supporting the generalizability of the design. The optimal map-absent performance was observed at N:T:T&M = 0.5:0.3:0.2. Increasing T&M led to over-reliance on map priors, slightly degrading temporal-prior performance. Reducing T&M, while avoiding such over-reliance, could still harm temporal modeling if map priors provide useful supervisory signals. Thus, insufficient map involvement also impaired performance. When T&M was entirely absent, the model reverted to a temporal-only mode.

**Qualitative Analysis** Figure 3 shows predictions and priors from Uni-PrevPredMap, comparing results with and without corrupted HD maps in occlusion, rainy, and night conditions. Purple shading highlights the differences. Without corrupted maps, the model fails to accurately predict map elements in these challenging environments, whereas the incorporation of corrupted HD maps enables effective use of complementary priors, resulting in significantly clearer and more precise predictions. Additional examples can be found in Appendix A.7.

#### 4.4. Limitations and Future Work

Based on current understanding, Uni-PrevPredMap’s limitations and future work focus on three key aspects. (1) The 3D global map uses height data only for filtering, not prior generation, due to the high latency of 3D rasterization, and limited vertical diversity in existing benchmarks. Future work should focus on efficient 3D representations and richer 3D datasets. (2) Evaluation relied on simulated perturbations; a main limitation is the absence of real corrupted maps (e.g., from outdated or crowdsourced sources). Building standardized real-corruption benchmarks is an essential next step. (3) Integrating temporal priors with complementary information shows promise for end-to-end autonomous driving. Map construction inherently functions as a fundamental auxiliary task, while 3D object detection could leverage vehicle-infrastructure cooperation to acquire prior information about surrounding entities. Incorporating such complementary priors may enhance robustness and safety in complex scenarios.

## 5. Conclusion

This paper introduces Uni-PrevPredMap, a unified prior-informed framework for online vectorized HD map construction that integrates two complementary prior sources: previous predictions and corrupted HD maps. The framework employs a tri-mode paradigm ensuring operational consistency across non-prior, temporal-prior, and temporal-map-fusion modes. This tri-mode paradigm simultaneously liberates the system from ideal map assumptions while maintaining robust performance in both map-present and map-absent scenarios. Complementing this, we develop a

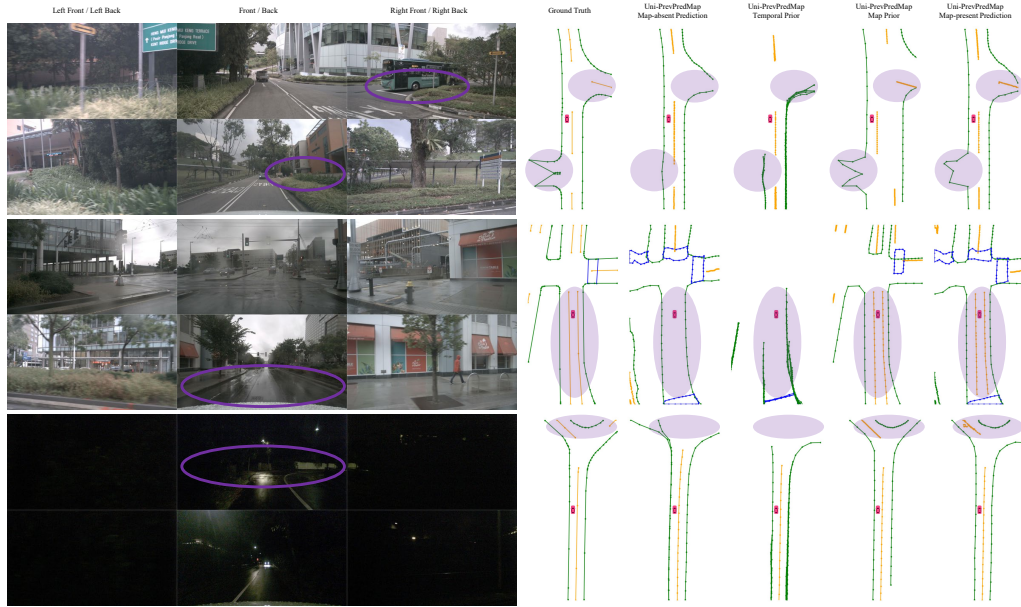


Figure 3. Comparison of predictions by Uni-PrevPredMap with versus without corrupted HD maps, with differences highlighted in purple shading across occlusion, rainy, and night scenarios. Corresponding priors are illustrated to demonstrate their influence. Green, orange, and blue lines represent road boundaries, lane dividers, and pedestrian crossings, respectively.

tile-indexed 3D vectorized global map processor enabling efficient 3D prior updates, compact storage, and real-time retrieval. Uni-PrevPredMap achieves state-of-the-art performance on established online vectorized HD map benchmarks without map priors. When processing corrupted HD maps, it demonstrates robust error-resilient fusion capabilities that empirically validate the synergistic complementarity between temporal predictions and imperfect map data. We anticipate this work will provide valuable insights for autonomous driving perception systems.

## References

- [1] Samuel M Bateman, Ning Xu, H Charles Zhao, Yael Ben Shalom, Vince Gong, Greg Long, and Will Maddern. Exploring real world map change generalization of prior-informed hd map prediction models. In *Proceedings of the IEEE/CVF Conference on Computer Vision and Pattern Recognition*, pages 4568–4578, 2024. 1, 3
- [2] Holger Caesar, Varun Bankiti, Alex H Lang, Sourabh Vora, Venice Erin Liong, Qiang Xu, Anush Krishnan, Yu Pan, Giancarlo Baldan, and Oscar Beijbom. nuscenes: A multi-modal dataset for autonomous driving. In *Proceedings of the IEEE/CVF conference on computer vision and pattern recognition*, pages 11621–11631, 2020. 5
- [3] Jiacheng Chen, Yuefan Wu, Jiaqi Tan, Hang Ma, and Yasutaka Furukawa. Maptracker: Tracking with strided memory fusion for consistent vector hd mapping. In *European Conference on Computer Vision*, pages 90–107. Springer, 2024. 1, 3, 5, 6, 14, 16
- [4] Shaoyu Chen, Tianheng Cheng, Xinggang Wang, Wenming Meng, Qian Zhang, and Wenyu Liu. Efficient and robust 2d-to-bev representation learning via geometry-guided kernel transformer. *arXiv preprint arXiv:2206.04584*, 2022. 2
- [5] Sehwan Choi, Jungho Kim, Hongjae Shin, and Jun Won Choi. Mask2map: Vectorized hd map construction using bird’s eye view segmentation masks. In *European Conference on Computer Vision*, pages 19–36. Springer, 2024. 2, 5, 6, 14, 16
- [6] Wenjie Ding, Limeng Qiao, Xi Qiu, and Chi Zhang. Pivotnet: Vectorized pivot learning for end-to-end hd map construction. In *Proceedings of the IEEE/CVF International Conference on Computer Vision*, pages 3672–3682, 2023. 2
- [7] Wenjie Gao, Jiawei Fu, Yanqing Shen, Haodong Jing, Shitao Chen, and Nanning Zheng. Complementing onboard sensors with satellite maps: a new perspective for hd map construction. In *2024 IEEE International Conference on Robotics and Automation (ICRA)*, pages 11103–11109. IEEE, 2024. 3
- [8] Xiaoshuai Hao, Ruikai Li, Hui Zhang, Dingzhe Li, Rong Yin, Sangil Jung, Seung-In Park, ByungIn Yoo, Haimei Zhao, and Jing Zhang. Mapdistill: Boosting efficient camera-based hd map construction via camera-lidar fusion model distillation. In *European Conference on Computer Vision*, pages 166–183. Springer, 2024. 2
- [9] Kaiming He, Xiangyu Zhang, Shaoqing Ren, and Jian Sun. Deep residual learning for image recognition. In *Proceedings of the IEEE conference on computer vision and pattern recognition*, pages 770–778, 2016. 5
- [10] Haotian Hu, Fanyi Wang, Yaonong Wang, Laifeng Hu, Jingwei Xu, and Zhiwang Zhang. Admap: Anti-disturbance

- framework for reconstructing online vectorized hd map. *arXiv preprint arXiv:2401.13172*, 2024. **2**
- [11] Haotian Hu, Jingwei Xu, Fanyi Wang, Toyota Li, Yaonong Wang, Laifeng Hu, and Zhiwang Zhang. Fastmap: Fast queries initialization based vectorized hd map reconstruction framework. *arXiv preprint arXiv:2503.05492*, 2025. **6**
- [12] Junjie Huang and Guan Huang. Bevpoolv2: A cutting-edge implementation of bevnet toward deployment. *arXiv preprint arXiv:2211.17111*, 2022. **5**
- [13] Bo Jiang, Shaoyu Chen, Qing Xu, Bencheng Liao, Jiajie Chen, Helong Zhou, Qian Zhang, Wenyu Liu, Chang Huang, and Xinggong Wang. Vad: Vectorized scene representation for efficient autonomous driving. In *Proceedings of the IEEE/CVF International Conference on Computer Vision*, pages 8340–8350, 2023. **1**
- [14] Zhou Jiang, Zhenxin Zhu, Pengfei Li, Huan-ang Gao, Tianyuan Yuan, Yongliang Shi, Hang Zhao, and Hao Zhao. P-mapnet: Far-seeing map generator enhanced by both sdmap and hdmap priors. *IEEE Robotics and Automation Letters*, 2024. **1, 3, 6**
- [15] Nayeon Kim, Hongje Seong, Daehyun Ji, and Sujin Jang. Unveiling the hidden: Online vectorized hd map construction with clip-level token interaction and propagation. *Advances in Neural Information Processing Systems*, 37:111358–111381, 2025. **1, 3, 6, 14, 15**
- [16] Qi Li, Yue Wang, Yilun Wang, and Hang Zhao. Hdmapnet: An online hd map construction and evaluation framework. In *2022 International Conference on Robotics and Automation (ICRA)*, pages 4628–4634. IEEE, 2022. **2, 5**
- [17] Tianyu Li, Peijin Jia, Bangjun Wang, Li Chen, Kun Jiang, Junchi Yan, and Hongyang Li. Laneseget: Map learning with lane segment perception for autonomous driving. In *ICLR*, 2024. **2**
- [18] Zhiqi Li, Wenhai Wang, Hongyang Li, Enze Xie, Chonghao Sima, Tong Lu, Yu Qiao, and Jifeng Dai. Bevformer: Learning bird’s-eye-view representation from multi-camera images via spatiotemporal transformers. In *European conference on computer vision*, pages 1–18. Springer, 2022. **2**
- [19] Bencheng Liao, Shaoyu Chen, Xinggong Wang, Tianheng Cheng, Qian Zhang, Wenyu Liu, and Chang Huang. Maptr: Structured modeling and learning for online vectorized hd map construction. In *International Conference on Learning Representations*, 2023. **1, 2, 5**
- [20] Bencheng Liao, Shaoyu Chen, Yunchi Zhang, Bo Jiang, Qian Zhang, Wenyu Liu, Chang Huang, and Xinggong Wang. Maptrv2: An end-to-end framework for online vectorized hd map construction. *International Journal of Computer Vision*, pages 1–23, 2024. **2, 6**
- [21] Ruixin Liu and Zejian Yuan. Compact hd map construction via douglas-peucker point transformer. In *Proceedings of the AAAI Conference on Artificial Intelligence*, volume 38, pages 3702–3710, 2024. **2**
- [22] Xiaolu Liu, Song Wang, Wentong Li, Ruizi Yang, Junbo Chen, and Jianke Zhu. Mgmmap: Mask-guided learning for online vectorized hd map construction. In *Proceedings of the IEEE/CVF Conference on Computer Vision and Pattern Recognition*, pages 14812–14821, 2024. **2**
- [23] Yicheng Liu, Tianyuan Yuan, Yue Wang, Yilun Wang, and Hang Zhao. Vectormapnet: End-to-end vectorized hd map learning. In *International Conference on Machine Learning*, pages 22352–22369. PMLR, 2023. **2, 5**
- [24] Zihao Liu, Xiaoyu Zhang, Guangwei Liu, Ji Zhao, and Ningyi Xu. Leveraging enhanced queries of point sets for vectorized map construction. In *European Conference on Computer Vision*, pages 461–477. Springer, 2024. **2**
- [25] Katie Z Luo, Xinshuo Weng, Yan Wang, Shuang Wu, Jie Li, Kilian Q Weinberger, Yue Wang, and Marco Pavone. Augmenting lane perception and topology understanding with standard definition navigation maps. In *2024 IEEE International Conference on Robotics and Automation (ICRA)*, pages 4029–4035. IEEE, 2024. **3**
- [26] Zhongxing Ma, Shuang Liang, Yongkun Wen, Weixin Lu, and Guowei Wan. Roadpainter: Points are ideal navigators for topology transformer. In *European Conference on Computer Vision*, pages 179–195. Springer, 2024. **2**
- [27] Thomas Monninger, Md Zafar Anwar, Stanislaw Antol, Steffen Staab, and Sihao Ding. Augmapnet: Improving spatial latent structure via bev grid augmentation for enhanced vectorized online hd map construction. *arXiv preprint arXiv:2503.13430*, 2025. **15**
- [28] Bowen Pan, Jiankai Sun, Ho Yin Tiga Leung, Alex Andonian, and Bolei Zhou. Cross-view semantic segmentation for sensing surroundings. *IEEE Robotics and Automation Letters*, 5(3):4867–4873, 2020. **2**
- [29] Nan Peng, Xun Zhou, Mingming Wang, Xiaojun Yang, Songming Chen, and Guisong Chen. Prevpredmap: Exploring temporal modeling with previous predictions for online vectorized hd map construction. *arXiv preprint arXiv:2407.17378*, 2024. **1, 2, 3, 6**
- [30] Limeng Qiao, Wenjie Ding, Xi Qiu, and Chi Zhang. End-to-end vectorized hd-map construction with piecewise bezier curve. In *Proceedings of the IEEE/CVF Conference on Computer Vision and Pattern Recognition*, pages 13218–13228, 2023. **2, 14**
- [31] Anqi Shi, Yuze Cai, Xiangyu Chen, Jian Pu, Zeyu Fu, and Hong Lu. Globalmapnet: An online framework for vectorized global hd map construction. *arXiv preprint arXiv:2409.10063*, 2024. **2**
- [32] Rémy Sun, Li Yang, Diane Lingrand, and Frédéric Precioso. Mind the map! accounting for existing map information when estimating online hdm maps from sensor data. *arXiv preprint arXiv:2311.10517*, 2023. **1, 3, 6**
- [33] Rongxuan Wang, Xin Lu, Xiaoyang Liu, Xiaoyi Zou, Tongyi Cao, and Ying Li. Priormapnet: Enhancing online vectorized hd map construction with priors. *arXiv preprint arXiv:2408.08802*, 2024. **6, 14, 15**
- [34] Shuo Wang, Fan Jia, Weixin Mao, Yingfei Liu, Yucheng Zhao, Zehui Chen, Tiancai Wang, Chi Zhang, Xiangyu Zhang, and Feng Zhao. Stream query denoising for vectorized hd-map construction. In *European Conference on Computer Vision*, pages 203–220. Springer, 2024. **1, 2, 14, 15**
- [35] Benjamin Wilson, William Qi, Tanmay Agarwal, John Lambert, Jagjeet Singh, Siddhesh Khandelwal, Bowen

- Pan, Ratnesh Kumar, Andrew Hartnett, Jhony Kaesemodel Pontes, et al. Argoverse 2: Next generation datasets for self-driving perception and forecasting. *arXiv preprint arXiv:2301.00493*, 2023. 5
- [36] Hang Wu, Zhenghao Zhang, Siyuan Lin, Tong Qin, Jin Pan, Qiang Zhao, Chunjing Xu, and Ming Yang. Blos-bev: Navigation map enhanced lane segmentation network, beyond line of sight. In *2024 IEEE Intelligent Vehicles Symposium (IV)*, pages 3212–3219. IEEE, 2024. 3
- [37] Xuan Xiong, Yicheng Liu, Tianyuan Yuan, Yue Wang, Yilun Wang, and Hang Zhao. Neural map prior for autonomous driving. In *Proceedings of the IEEE/CVF Conference on Computer Vision and Pattern Recognition*, pages 17535–17544, 2023. 3
- [38] Zhenhua Xu, Kwan-Yee K. Wong, and Hengshuang Zhao. Insmapper: Exploring inner-instance information for vectorized hd mapping. In *European Conference on Computer Vision*, pages 296–312. Springer, 2024. 2
- [39] Jing Yang, Minyue Jiang, Sen Yang, Xiao Tan, Yingying Li, Errui Ding, Hanli Wang, and Jingdong Wang. Mgmmapnet: Multi-granularity representation learning for end-to-end vectorized hd map construction. *arXiv preprint arXiv:2410.07733*, 2024. 6
- [40] Tianyuan Yuan, Yicheng Liu, Yue Wang, Yilun Wang, and Hang Zhao. Streammapnet: Streaming mapping network for vectorized online hd map construction. In *Proceedings of the IEEE/CVF Winter Conference on Applications of Computer Vision*, pages 7356–7365, 2024. 1, 2, 14, 15
- [41] Tianyuan Yuan, Yucheng Mao, Jiawei Yang, Yicheng Liu, Yue Wang, and Hang Zhao. Presight: Enhancing autonomous vehicle perception with city-scale nerf priors. In *European Conference on Computer Vision*, pages 323–339. Springer, 2024. 3
- [42] Xiaoyu Zhang, Guangwei Liu, Zihao Liu, Ningyi Xu, Yunhui Liu, and Ji Zhao. Enhancing vectorized map perception with historical rasterized maps. In *European Conference on Computer Vision*, pages 422–439. Springer, 2024. 1, 2, 3, 4, 6, 15
- [43] Zhixin Zhang, Yiyuan Zhang, Xiaohan Ding, Fusheng Jin, and Xiangyu Yue. Online vectorized hd map construction using geometry. In *European Conference on Computer Vision*, pages 73–90. Springer, 2024. 2
- [44] Yi Zhou, Hui Zhang, Jiaqian Yu, Yifan Yang, Sangil Jung, Seung-In Park, and ByungIn Yoo. Himap: Hybrid representation learning for end-to-end vectorized hd map construction. In *Proceedings of the IEEE/CVF Conference on Computer Vision and Pattern Recognition*, pages 15396–15406, 2024. 2, 6
- [45] Xi Zhu, Xiya Cao, Zhiwei Dong, Caifa Zhou, Qiangbo Liu, Wei Li, and Yongliang Wang. Nemo: Neural map growing system for spatiotemporal fusion in bird’s-eye-view and bdd-map benchmark. *arXiv preprint arXiv:2306.04540*, 2023. 3

## A. Appendix

---

### Algorithm 1: Tri-mode Paradigm during Training

---

**Input:** Mode sampling ratio  $R$ , global map  $G(i, j)$ , ego pose  $E$

**Output:** Temporal heatmap  $H_t$ , map heatmap  $H_m$

```

1  $H_t, H_m \leftarrow \text{zeros}()$ ;
2  $mode \leftarrow \text{sampleMode}(R)$ ;
3 if  $mode == \text{non-prior}$  then
4   | return  $H_t, H_m$ 
5 end
6 else
7   |  $V_t \leftarrow \text{retrieveVectors}(G(i, j), E)$ ;
8   |  $H_t \leftarrow \text{rasterizeToHeatmap}(V_t)$ ;
9   | if  $mode == \text{temporal-map-fusion}$  then
10  |   |  $V_m \leftarrow \text{retrieveVectors}(G(i, j), E)$ ;
11  |   |  $H_m \leftarrow \text{rasterizeToHeatmap}(V_m)$ ;
12  | end
13  | return  $H_t, H_m$ 
14 end

```

---

### A.1. Artificial HD Map Perturbations

We design six perturbation types to simulate real-world corruption and test robustness, including instance-level displacement, addition, and deletion alongside frame-level displacement, rotation, and scaling. Comparative visualizations of these perturbations are provided in Figure 4.

**Instance-level displacement** applies distinct displacement magnitudes to randomly selected map vector subsets per frame, sampling magnitudes uniformly over a specified range. For Uni-PrevPredMap training, this range is specifically set to  $[-6, 6]$  meters, stochastically displacing statistically averaged 50% of map vectors with mean 3-meter displacement approximating standard lane width specifications. This configuration simulates common infrastructure modifications including divider addition/removal, boundary adjustments, and pedestrian crossing relocation through controlled perturbation protocols.

**Instance-level addition** incorporates  $n \sim U[0, 10]$  non-existent elements per frame to simulate real-world map element removals such as road closures or infrastructure decommissioning. These elements are randomly sampled from all map elements across the entire validation dataset, ensuring structurally diverse yet geometrically plausible configurations.

**Instance-level deletion** removes  $n \sim U[0, \min(10, n_{gt})]$  existing elements per frame to simulate unmapped construction scenarios, where  $n_{gt}$  denotes the map element count in the corresponding frame. Given that nuScenes datasets average fewer than 10 map elements per

frame, this configuration statistically deletes an average of 50% of map vectors per frame.

**Frame-level displacement** uniformly displaces all map vectors per frame by sampling displacement magnitudes from a uniform distribution over a specified range, specifically simulating positional errors within pose misalignment scenarios.

**Frame-level rotation** uniformly rotates all map vectors per frame through sampling  $\theta \sim U[-15^\circ, 15^\circ]$ , specifically simulating orientation errors within pose misalignment scenarios.

**Frame-level scaling** uniformly scales all map vectors per frame through sampling  $s \sim U[0.8, 1.2]$ , inherently generating displacement as a geometric coupling effect due to coordinate transformation.

### A.2. Refreshment and Retrieval of Tile-indexed 3D Vectorized Global Map Processor

Algorithms 2 and 3 illustrate the workflows of the refreshment and retrieval modules, respectively.

---

### Algorithm 2: Refreshment Algorithm

---

**Input:** Global map  $G(i, j)$ , predicted map vectors  $V(k)$ , confidence threshold  $\tau$ , ego pose  $E$

**Output:** Updated global map  $G(i, j)$

```

1  $i, j \leftarrow \text{getTileIndex}(E)$ ;
2 for each map vector  $k$  in  $V(k)$  do
3   | if  $\text{confidence}(V(k)) > \tau$  then
4   |   |  $\hat{V}(k) \leftarrow \text{egoToGlobal}(V(k), E)$ ;
5   |   |  $G(i, j) \leftarrow G(i, j) \parallel \hat{V}(k)$ ;
6   | end
7 end

```

---

**Refreshment** mapping between tile indices  $(i, j)$  and UTM coordinates  $(UTM_{east}, UTM_{north})$  is defined as:

$$(i, j) = (UTM_{east}, UTM_{north}) // l, \quad (1)$$

where  $l$  denotes the long side length of the perception range.

**Retrieval** mapping between tile indices  $\{(i, j) \mid i \in I, j \in J\}$  and UTM coordinates  $(UTM_{east}, UTM_{north})$  is defined as:

$$I = \begin{cases} (i_t - 1, i_t) & \text{if } UTM_{east} \% l < l/2 \\ (i_t) & \text{if } UTM_{east} \% l = l/2 \\ (i_t, i_t + 1) & \text{if } UTM_{east} \% l > l/2 \end{cases}, \quad (2)$$

$$J = \begin{cases} (j_t - 1, j_t) & \text{if } UTM_{north} \% l < l/2 \\ (j_t) & \text{if } UTM_{north} \% l = l/2 \\ (j_t, j_t + 1) & \text{if } UTM_{north} \% l > l/2 \end{cases}, \quad (3)$$

where  $i_t$  and  $j_t$  denote the indices of target tile. As depicted in Figure 5, the adjacency selection is determined by the spatial position of the vehicle's UTM coordinates relative to the target tile boundaries.

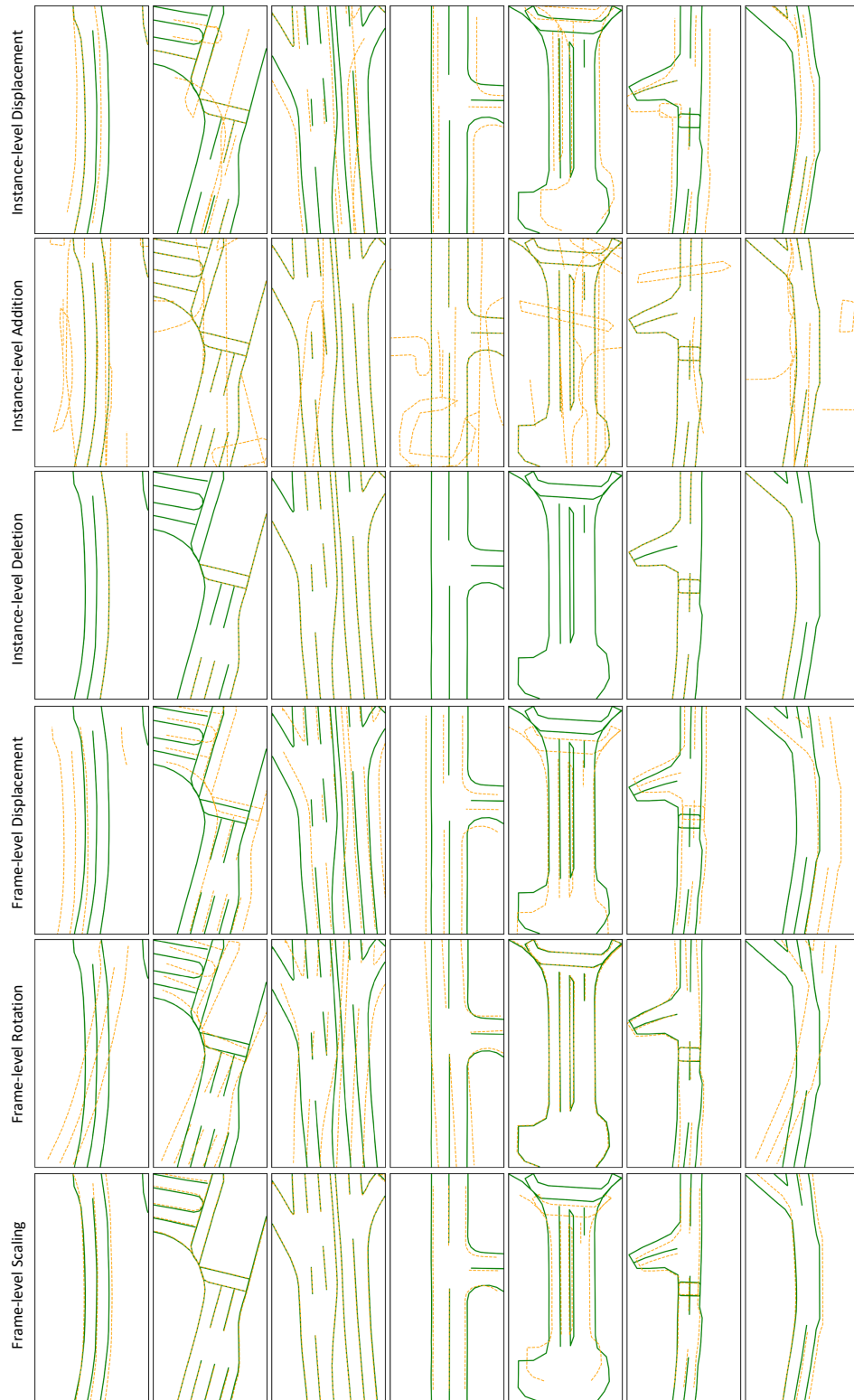


Figure 4. Comparison of artificially perturbed HD maps (orange dashed) vs. ground truth annotations (green solid) with identical random seeds ensuring reproducible and fair comparisons.

---

**Algorithm 3: Retrieval Algorithm**

---

**Input:** Global map  $G(i, j)$ , ego pose  $E$ , perception range  $R$   
**Output:** Retrieved map vectors  $V(k)$

```
1  $i, j \leftarrow \text{getTileIndex}(E)$ ;  
2  $list_i, list_j \leftarrow \text{getAdjacentTileIndexList}(E, R)$ ;  
3  $list_i, list_j \leftarrow list_i \parallel i, list_j \parallel j$ ;  
4 for each  $i$  in  $list_i$  do  
5   for each  $j$  in  $list_j$  do  
6      $\tilde{V}(\hat{k}) \leftarrow$   
        $\text{filterByPerceptionRange}(G(i, j), R)$ ;  
7      $V(\hat{k}) \leftarrow \text{globalToEgo}(\tilde{V}(\hat{k}), E)$ ;  
8      $V(k) \leftarrow V(k) \parallel V(\hat{k})$ ;  
9   end  
10 end
```

---

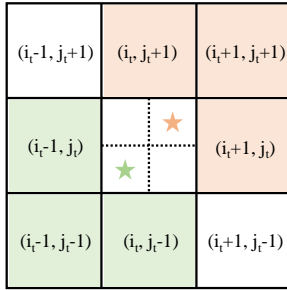


Figure 5. Visualization of adjacency selection during retrieval. The central grid indicates the target tile with indices  $(i_t, j_t)$ . Orange and green star markers denote distinct vehicle UTM coordinate positions within the target tile, with corresponding shaded grids indicating respective adjacent tiles.

### A.3. Comparison on Geographically Non-Overlapping NuScenes and ArgoVerse2

StreamMapNet [40] proposes a geographically non-overlapping dataset partitioning strategy for nuScenes and ArgoVerse2. The comparative performance of Uni-PrevPredMap under this configuration is detailed in Table 10. As evidenced by Table 10, Uni-PrevPredMap maintains superior performance in both temporal-prior and temporal-map-fusion-prior operational modes under the geographically non-overlapping data distribution paradigm.

### A.4. Comparison on NuScenes and ArgoVerse2 with Extended Perception Range

Following experimental configurations from established methods [15, 33, 34], the extended perception range adopts 50m front/rear and 25m lateral coverage relative to the vehicle. Evaluation employs Chamfer Distance-based average precision (AP) across three thresholds:  $\{1.0, 1.5, 2.0\}$ m. As

evidenced in Table 11, Uni-PrevPredMap sustains superior performance under extended perception range across both temporal-prior and temporal-map-fusion-prior operational modes.

### A.5. Performance Comparison on Challenging Scenarios of NuScenes Dataset

Table 12 presents quantitative evaluation of corner cases across challenging scenarios including occlusion (dynamic objects within 2.5m of ego vehicle per MapUnveiler [15]) and adverse weather conditions (cloudy, rainy, night scenarios following BeMapNet [30] criteria). Compared to state-of-the-art open-source methods Mask2Map [5] and MapTracker [3], Uni-PrevPredMap consistently outperforms in occlusion, cloudy, and night environments despite a marginal 1 mAP decrease in rainy conditions primarily attributed to MapTracker’s temporal BEV feature aggregation. Crucially, Uni-PrevPredMap demonstrates significant robustness with corrupted map inputs, achieving over 3.6 mAP improvement compared to map-absent operation.

### A.6. Impact of Refreshment Threshold

The tile-indexed 3D vectorized global map processor enables automatic updating of predicted vectors (confidence  $>$  refreshment threshold) to their corresponding geolocation tiles, eliminating complex and time-consuming post-processing operations. As shown in Table 13, threshold adjustments during training approximately induce  $\pm 1.0$  mAP variation, suggesting potential systematic fluctuations inherent in post-processing pipelines. The tile-indexed 3D vectorized global map processor allows concentrated research efforts on the unified framework while maintaining operational robustness and retrieval efficiency.

### A.7. Computational Cost Analysis of Tile-indexed 3D Vectorized Global Map Processor

The computational workflow of the tile-indexed 3D vectorized global map processor comprises three main stages: retrieval, rasterization, and refreshment. First, the retrieval module queries the global tile-based storage to fetch relevant map vectors, filters them, and transforms them into the ego vehicle’s coordinate frame. These vectors are then rasterized into BEV heatmaps. Lastly, the refreshment module converts the predicted vectors back to global coordinates and stores them in the global map. As summarized in Table 14, the tile-indexing mechanism keeps the combined latency of the retrieval and refreshment stages low (approximately 5 ms). The rasterization step constitutes the most computationally intensive part of the process. Overall, the processor introduces a manageable increase in total inference time.

Table 10. Comparison on geographically non-overlapping nuScenes and ArgoVerse2.

Dataset	Method	$AP_{div}$	$AP_{ped}$	$AP_{bou}$	mAP
NuScenes	StreamMapNet [40]	30.1	29.6	41.9	33.9
	HRMapNet [42]	30.3	36.9	44.0	37.1
	MapUnveiler [15]	26.5	<b>43.2</b>	48.7	39.4
	AugMapNet [27]	30.3	39.4	45.3	38.3
	Uni-PrevPredMap	<b>36.1</b>	28.5	<b>54.4</b>	<b>39.7</b>
	Uni-PrevPredMap*	58.2	32.6	66.7	52.5
ArgoVerse2 (2d)	StreamMapNet [40]	55.9	56.9	61.4	57.1
	HRMapNet [42]	58.3	60.1	66.0	61.5
	AugMapNet [27]	57.4	57.4	61.6	58.8
	Uni-PrevPredMap	<b>64.9</b>	<b>65.2</b>	<b>70.7</b>	<b>67.0</b>
	Uni-PrevPredMap*	75.4	71.2	78.9	75.2
	ArgoVerse2 (3d)	Uni-PrevPredMap	63.4	64.1	70.5
Uni-PrevPredMap*		74.2	70.7	79.4	74.8

Table 11. Comparison on nuScenes and ArgoVerse2 with extended perception range.

Dataset	Method	$AP_{div}$	$AP_{ped}$	$AP_{bou}$	mAP
NuScenes	SQD-MapNet [34]	65.5	67.0	59.5	64.0
	MapUnveiler [15]	70.0	68.0	68.2	68.7
	PriorMapNet [33]	67.4	62.5	65.0	65.0
	Uni-PrevPredMap	<b>73.4</b>	<b>77.2</b>	<b>70.0</b>	<b>73.5</b>
	Uni-PrevPredMap*	87.3	83.0	77.5	82.6
	ArgoVerse2 (2d)	SQD-MapNet [34]	54.9	66.9	56.1
MapUnveiler [15]		67.1	69.7	59.3	65.4
Uni-PrevPredMap		<b>68.2</b>	<b>74.8</b>	<b>63.3</b>	<b>68.8</b>
Uni-PrevPredMap*		84.9	83.0	77.5	82.6
ArgoVerse2 (3d)		Uni-PrevPredMap	66.0	72.4	59.9
	Uni-PrevPredMap*	82.9	86.1	79.4	82.8

### A.8. Speed-accuracy Trade-off Comparison with SOTA methods

Figure 6 depicts the speed-accuracy trade-offs among state-of-the-art methods, underscoring our framework’s emphasis on robust, multi-mode performance. While prioritizing accuracy, our method’s inference speed could be further enhanced for high-speed applications, e.g., through parallelizing tile-indexed 3D vectorized global map processor, accelerating rasterization, or developing a lightweight variant.

### A.9. More Qualitative Results

Figures 7-12 demonstrate supplementary qualitative comparisons across both nuScenes and ArgoVerse2 datasets. Visualizations include nuScenes results under geographically non-overlapping split and extended perception range. Under all configurations, Uni-PrevPredMap<sup>3</sup>

(temporal-map-fusion-prior mode) effectively harnesses complementary priors to iteratively refine predictions while generating enhanced temporal priors, resulting in superior forecasting performance.

We also present the global prediction maps generated through consecutive-frame reasoning on the nuScenes dataset. Figures 13-15 depict top-down comparisons between the Ground Truth and three modes of our approach: UniPrevPredMap without prior, with temporal prior only, and with both temporal and map priors. The results visually confirm that the temporal prior markedly improves temporal smoothness, while the addition of map priors further reduces both false positives and false negatives.

### A.10. Broader Impact

While Uni-PrevPredMap integrates two complementary prior sources (previous predictions and corrupted HD maps)

Table 12. Performance comparison on challenging scenarios of nuScenes dataset.

Method	mAP	$mAP_{occlusion}$	$mAP_{cloudy}$	$mAP_{rainy}$	$mAP_{night}$
Mask2Map [5]	75.4	77.8	80.2	63.6	55.1
MapTracker [3]	76.1	73.9	79.3	<b>67.0</b>	51.9
Uni-PrevPredMap	<b>77.0</b>	<b>79.0</b>	<b>81.3</b>	66.0	<b>55.4</b>
Uni-PrevPredMap*	81.8	83.1	84.9	72.2	62.2

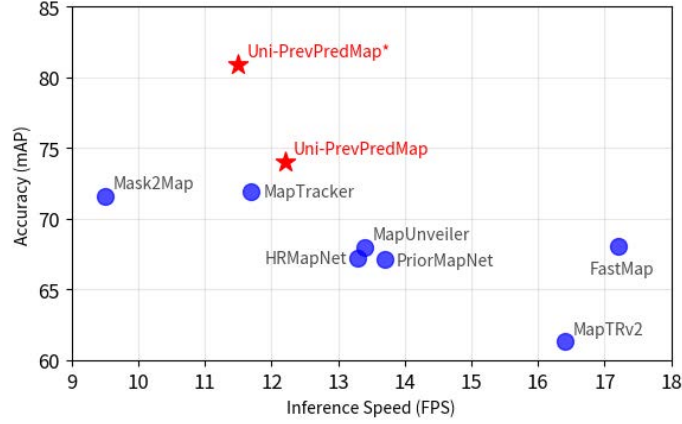


Figure 6. Speed-accuracy trade-off comparison with state-of-the-art methods.

Table 13. Impact of refreshment threshold. "T" and "M" denote temporal and map priors respectively.

Refreshment Threshold		mAP (T)	mAP (T&M)
@Training	@Inference		
0.3	0.5	72.9	80.3
	0.6	73.0	80.1
	0.7	72.8	80.0
0.4	0.7	73.7	81.0
	0.8	74.0	81.0
	0.9	74.0	80.9
0.5	0.5	72.6	79.2
	0.6	73.4	79.5
	0.7	73.2	79.6

Table 14. Computational cost analysis of tile-indexed 3D vectorized global map processor (measured on NVIDIA A6000). "Overall" indicates the total forward time of Uni-PrevPredMap.

Module	Time (w/o map)	Time (w/ map)
Retrieval	4.4 ms	5.1 ms
Rasterization	14.7 ms	18.9 ms
Refreshment	0.3 ms	0.3 ms
Overall	82.0 ms	87.0 ms

to optimize performance in online vectorized HD map construction, it does not guarantee error-free prediction of all map elements. Thus, implementing redundancy mechanisms for safety-critical applications remains essential.

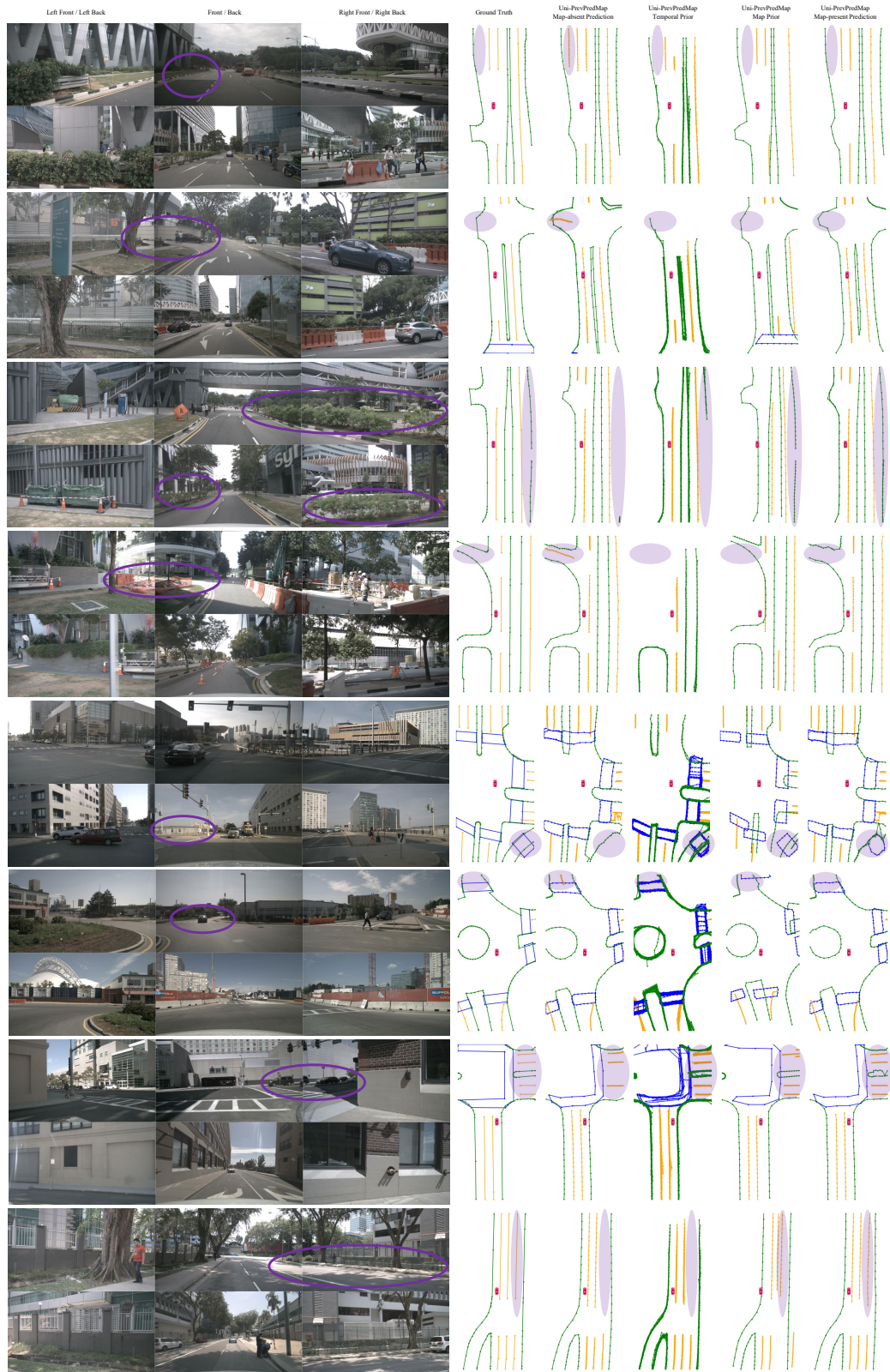


Figure 7. Additional qualitative results on the nuScenes dataset.

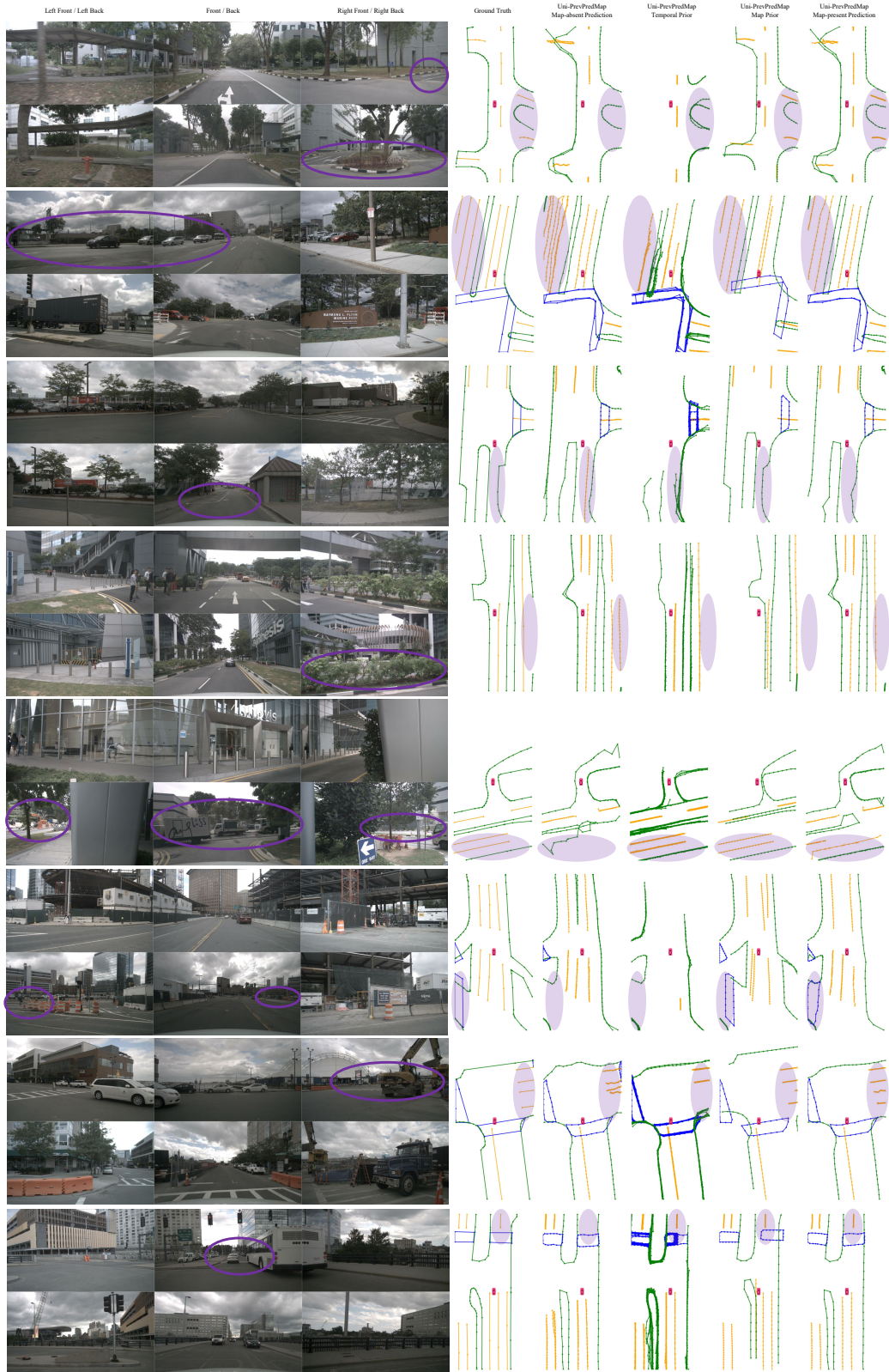


Figure 8. Additional qualitative results on the nuScenes dataset.

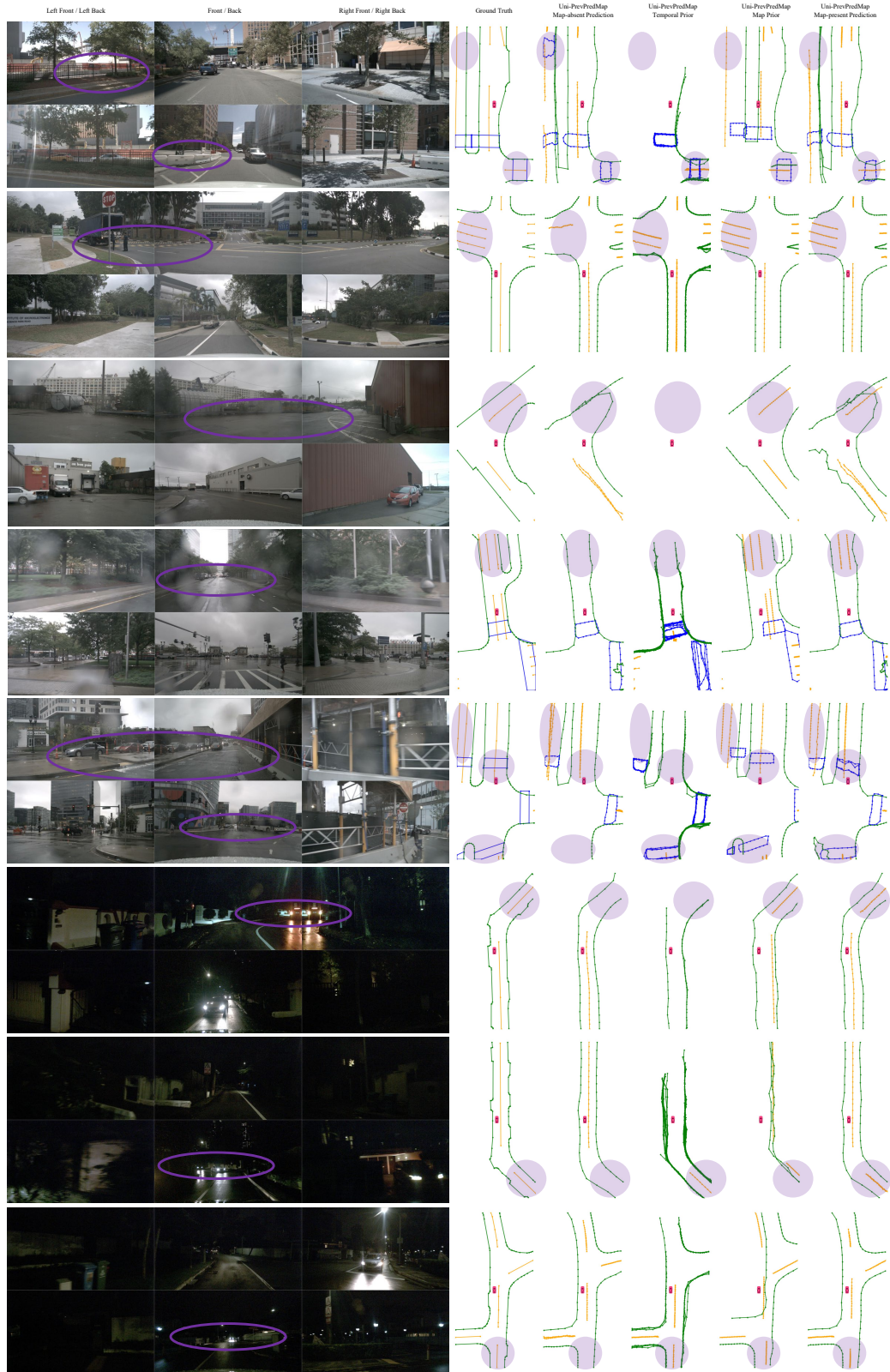


Figure 9. Additional qualitative results on the nuScenes dataset.

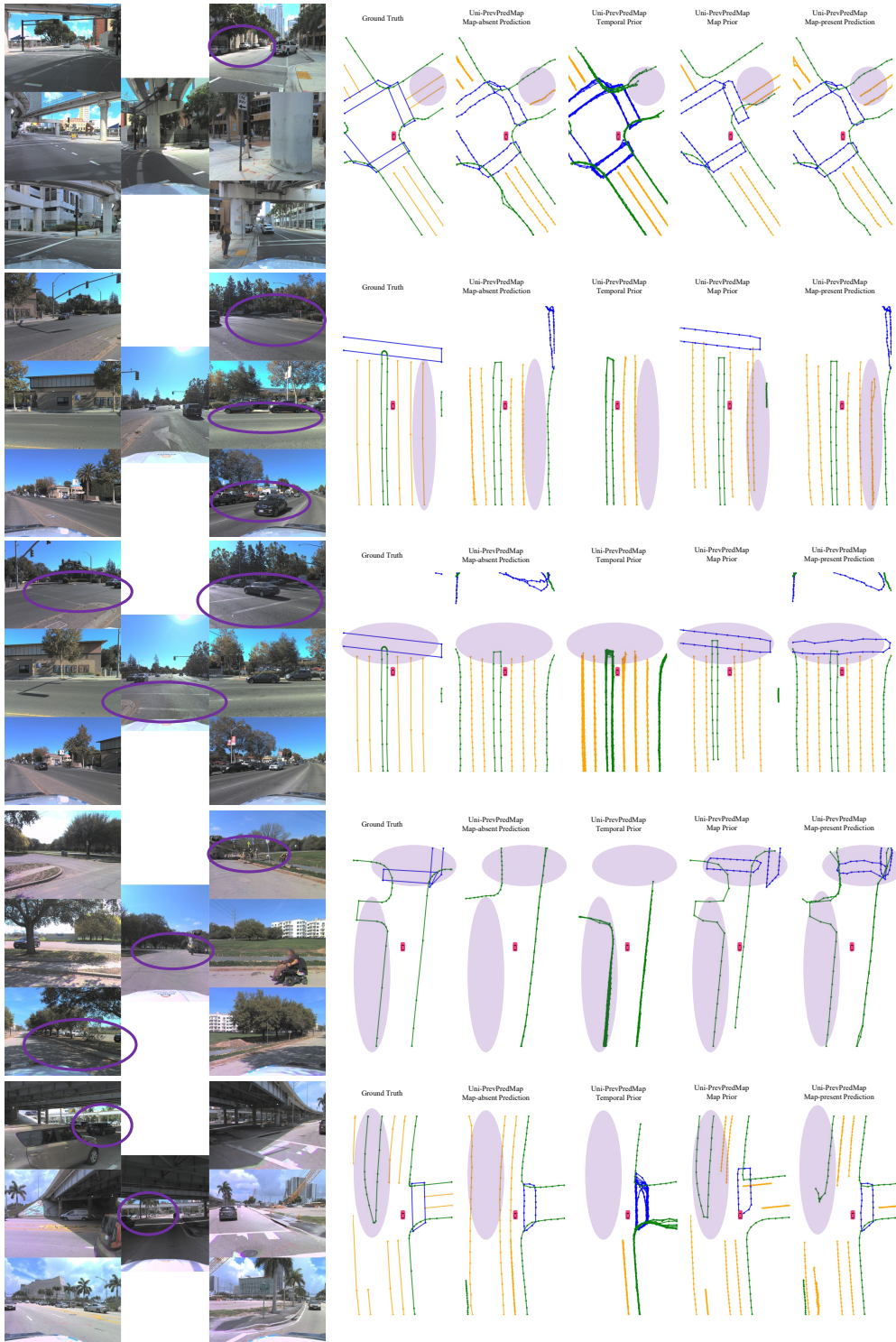


Figure 10. Additional qualitative results on the ArgoVerse2 dataset.

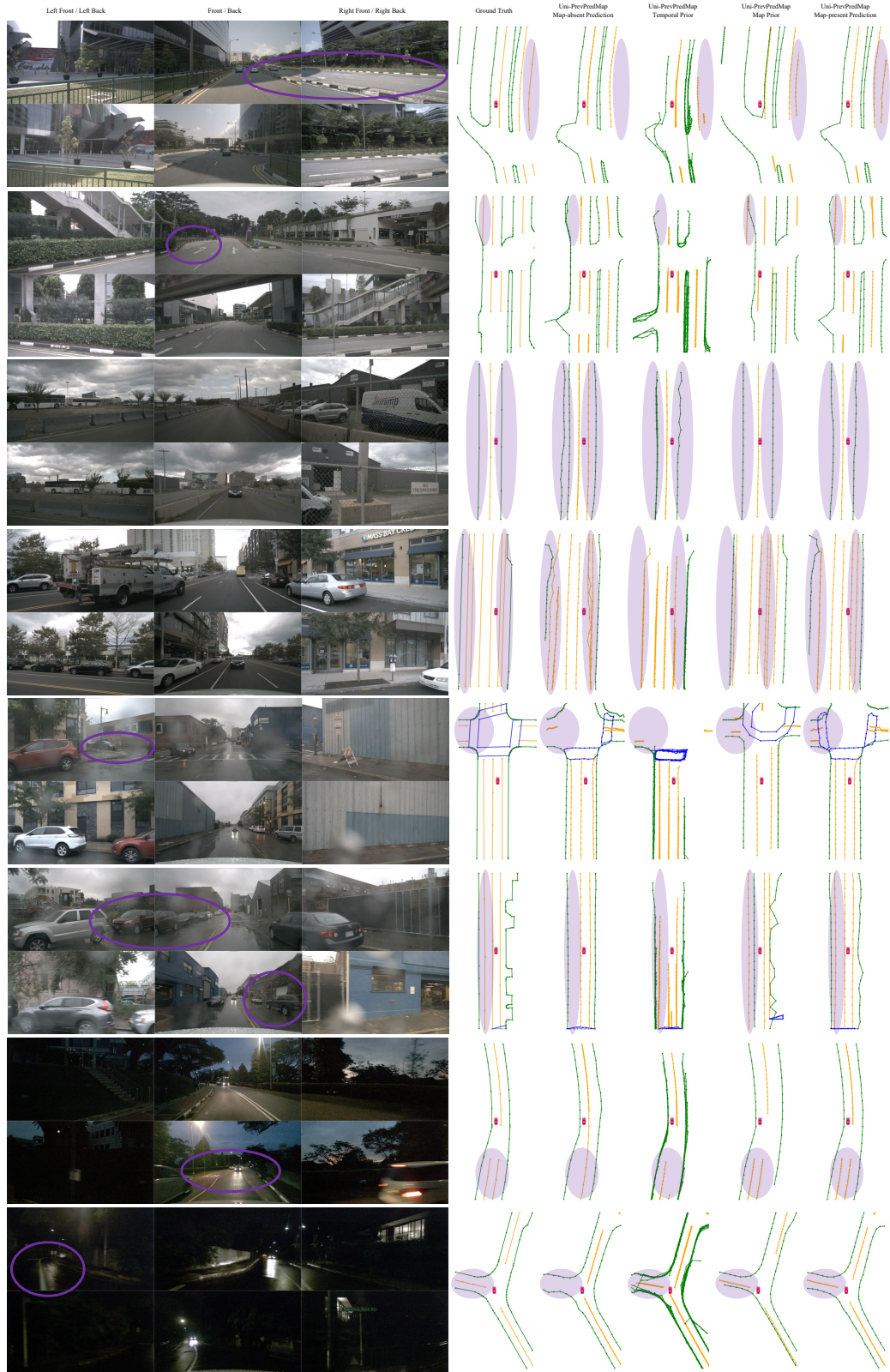


Figure 11. Additional qualitative results on the geographically non-overlapping nuScenes dataset.

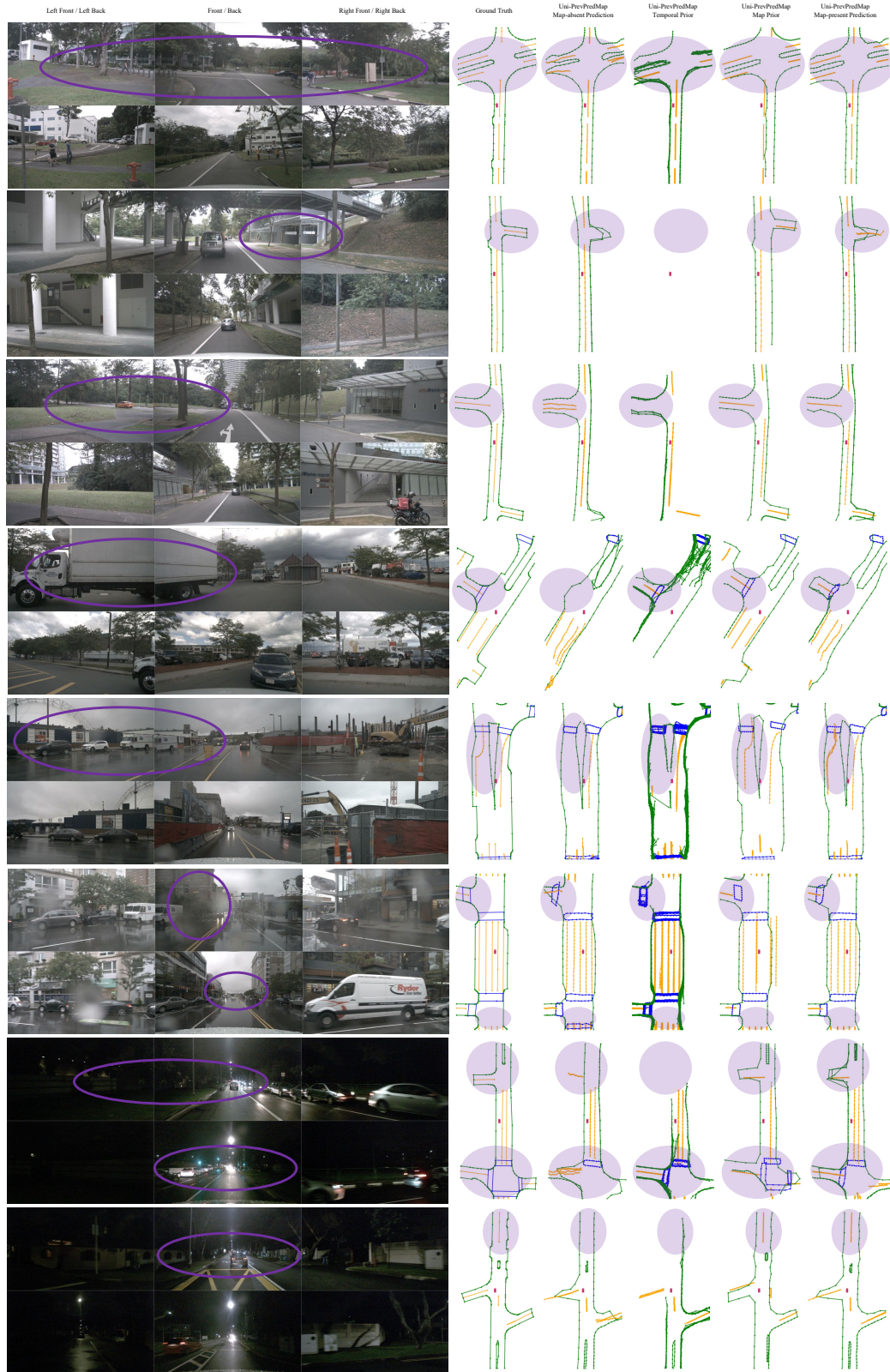


Figure 12. Additional qualitative results on the nuScenes dataset with the extended perception range.

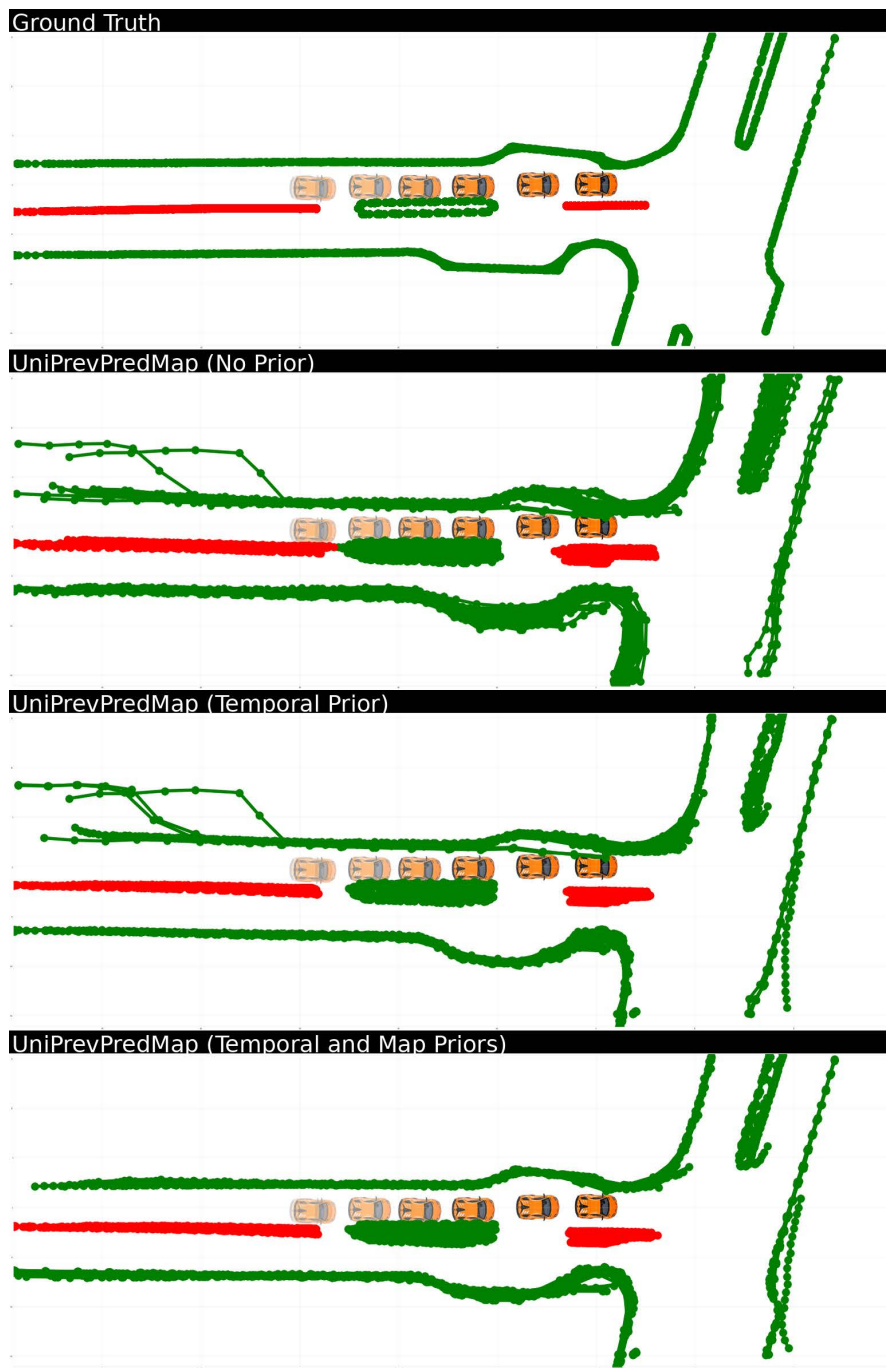


Figure 13. Additional qualitative results on the nuScenes dataset with global prediction maps.

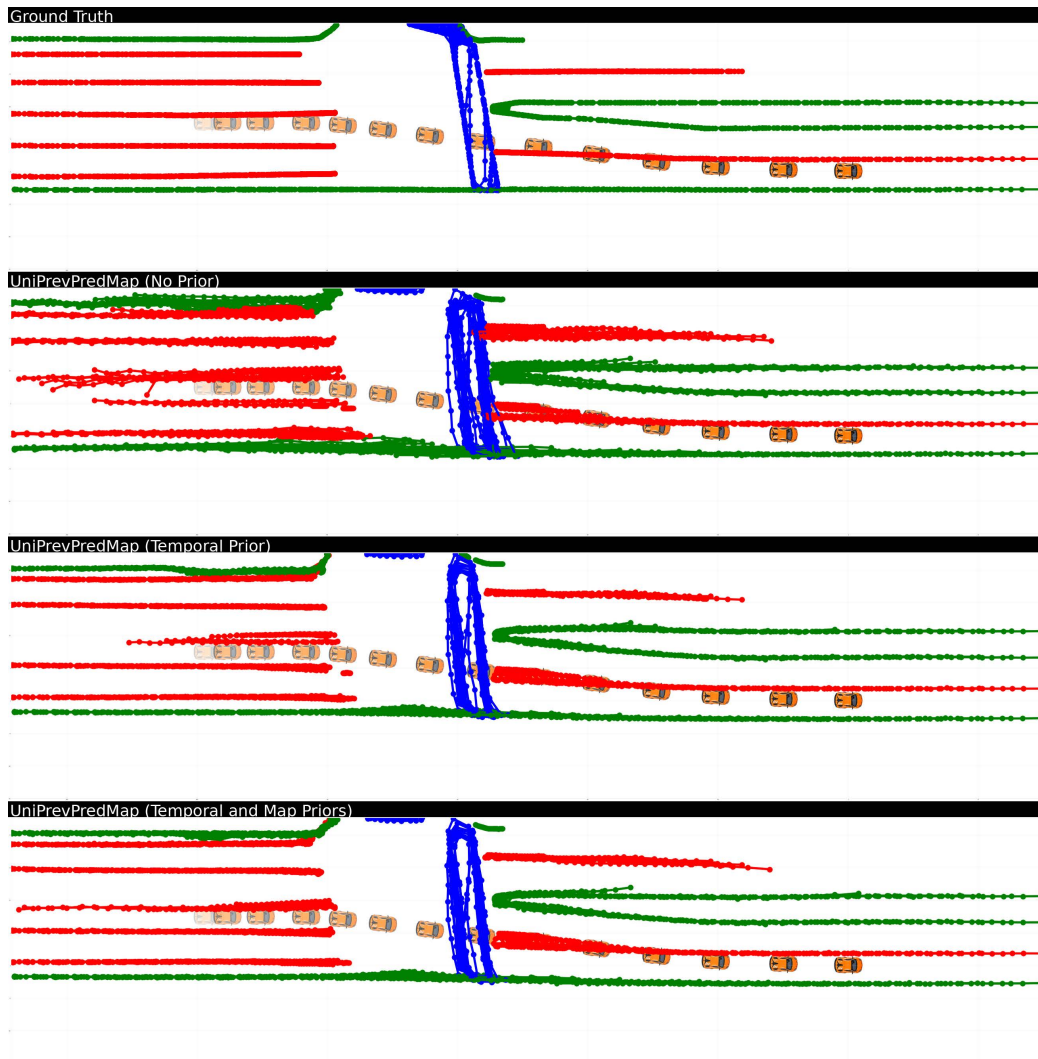


Figure 14. Additional qualitative results on the nuScenes dataset with global prediction maps.

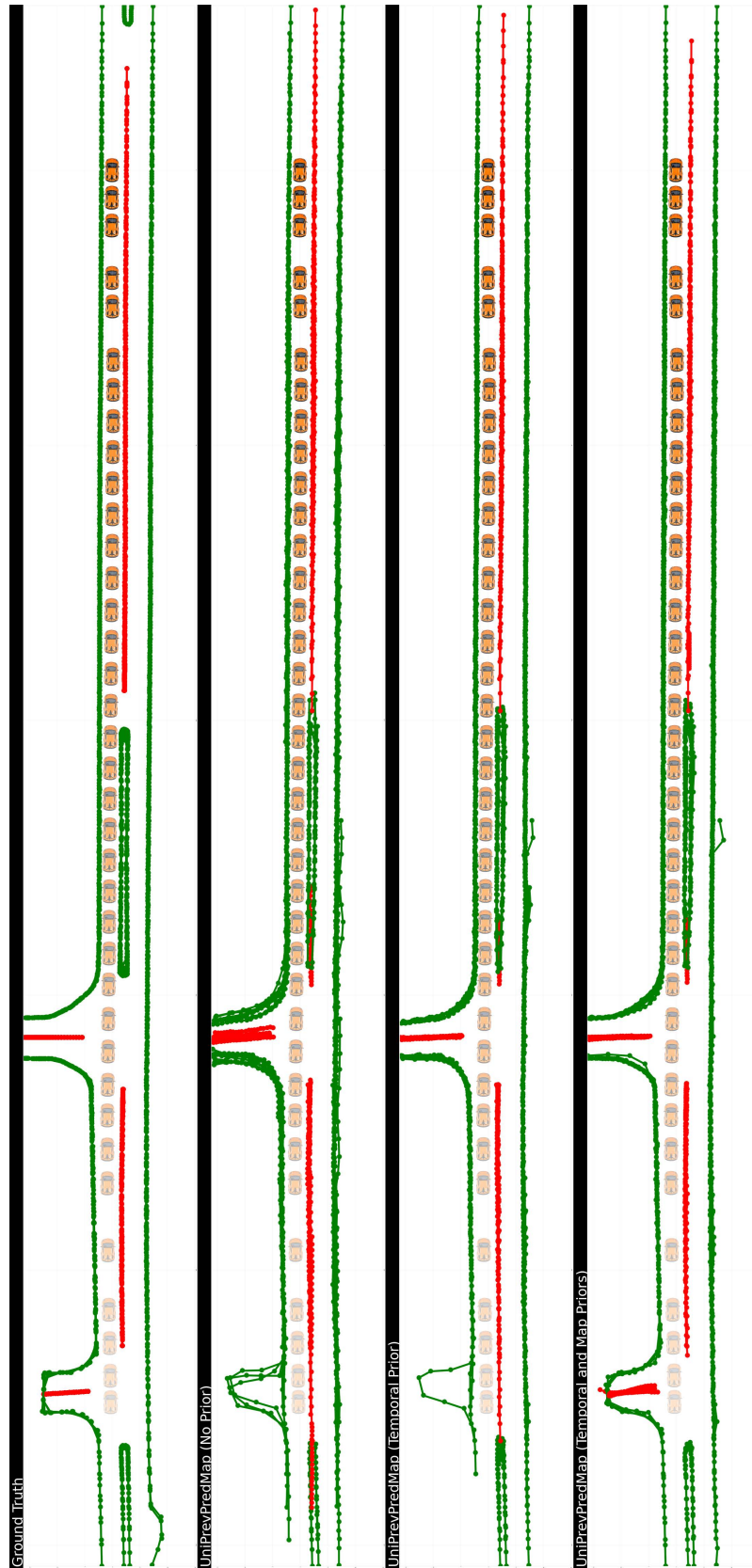


Figure 15. Additional qualitative results on the nuScenes dataset with global prediction maps.